HHS Public Access

Author manuscript

IEEE Robot Autom Lett. Author manuscript; available in PMC 2022 July 01.

Published in final edited form as:

IEEE Robot Autom Lett. 2021 July ; 6(3): 5292–5299. doi:10.1109/lra.2021.3073651.

A Soft Robotic Sleeve for Safer Colonoscopy Procedures

Max McCandless[1], **Arincheyan Gerald**[1], **Ashlyn Carroll**[1], **Hiroyuki Aihara**[2], **Sheila Russo**[*,1]

[1]Mechanical Engineering Department, Boston University, Boston, MA 02215 USA.

[2]Brigham and Women's Hospital, Harvard Medical School, Boston, MA 02115 USA.

Abstract

Colonoscopy is the gold standard for colorectal cancer diagnosis; however, limited instrument dexterity and no sensor feedback can hamper procedure safety and acceptance. We propose a soft robotic sleeve to provide sensor feedback and additional actuation capabilities to improve safety during navigation in colonoscopy. The robot can be mounted around current endoscopic instrumentation as a disposable "add-on", avoiding the need for dedicated or customized instruments and without disrupting current surgical workflow. We focus on design, finite element analysis, fabrication, and experimental characterization and validation of the soft robotic sleeve. The device integrates soft optical sensors to monitor contact interaction forces between the colon and the colonoscope and soft robotic actuators that can be automatically deployed if excessive force is detected, to guarantee pressure redistribution on a larger contact area of the colon. The system can be operated by a surgeon via a graphic user interface that displays contact force values and enables independent or coordinated pressurization of the soft actuators upon demand, in case deemed necessary to aid navigation or distend colon tissue.

Index Terms—

Medical Robots and Systems; Soft Robot Applications; Soft Robot Materials and Design; Soft Sensors and Actuators

I. INTRODUCTION

Colorectal cancer is the third most common cancer, with almost 1.4 million new cases and 694,000 deaths per year worldwide [1], 156,000 estimated new diagnoses and more than 54,000 deaths in the United States for 2020 [2]. Colonoscopy is a widespread minimally invasive surgical technique for colorectal cancer diagnosis. Current scopes have limited dexterity and no sensor feedback, hampering instrument controllability, thus making navigation a challenging task [3]. These technical limitations make colonoscopy poorly tolerated by patients, leading to low rates of compliance with screening guidelines [4]. Patient discomfort and intolerance are one of the main factors contributing to incomplete colonoscopy, which rates (4–25%) are associated with higher rates of colon cancer [5]. Plus,

*Corresponding author: russos@bu.edu.

severe adverse events (SAE) have been associated with colonoscopy, i.e. abdominal pain, perforation, and bleeding [6], [7]. Occurrence rates of SAEs are relatively rare (0.035–0.23%), but the patient population is quite extensive: the number of colonoscopies that will be performed in 2024 is estimated to be ~5–13 million in the US alone, which could result in between 1,750–30,000 SAEs per year, of which the 30-day mortality rate can exceed 4% of affected patients [8], [9]. Furthermore, in the US, 34.4% of colonoscopy procedures are performed with anesthesia, which has been shown to increase the risk of SAEs and post-operative complications within 30 days by 13% [10]. If colonoscopy was a gentle, tolerated, and safe procedure even without anesthesia, this could be beneficial to anesthesia-susceptible populations and expand the range of patients who would be eligible for the procedure, shorten patient recovery time, and potentially increase general rates of compliance [11].

Robotic solutions have been explored to enhance endoscopes capabilities [12]–[16]. A major drawback of such systems is the uncontrollability of the tension to the colon wall, caused by the lack of tactile feedback to the endoscopists [17], which can reach peak values of more than 40 N [18], leading to potential perforations. Soft robots represent a promising technology in this field because they are constructed from compliant materials with tensile properties similar to the human colon, thus can safely interact with delicate anatomical structures [19], [20]. Soft robotic solutions for colonoscopy include: inchworm-inspired robots to facilitate navigation [21], [22]; a pneumatic mechanism for self-propelled colonoscopy [23]; a disposable robotic endoscope based on bellow actuators [24]; a double-balloon system to ease access to the small intestine [25]; and soft-actuated foldable robots to enhance tissue manipulation and scope stabilization [26], [27]. In general, the majority of these systems are not compatible with commercial colonoscopes, thus requiring to re-learn new methods of performing surgery that is not cost-effective. Furthermore, only a few systems embed sensing to monitor tissue-endoscope interaction forces, including: an endoscope with pressure pads along its body to sense contact interactions with its environment [28]; a force visualization sensor for endoscope tip interaction monitoring [29]; and a haptic feedback system to estimate tip deformations from contact forces between the tissue and endoscope [30]. However, these systems only alert the user of certain force interactions without actively seeking to mitigate or counteract the excessive forces measured.

This paper presents a first proof-of-concept of a soft robotic sleeve (Fig. 1), designed as a disposable “add-on” endoscopic device, that can be wrapped around current endoscopic instrumentation and provide sensor feedback as well as additional actuation functionalities to improve navigation and safety in colonoscopy, avoiding the necessity for dedicated or customized instruments and without disrupting the current surgical workflow. The soft robot embeds distributed soft optical sensors to monitor the force exerted by the colonoscope onto surrounding tissue during navigation. If excessive force concentration is detected, embedded soft actuators can be inflated to guarantee pressure redistribution on a larger contact area.

II. Materials and Methods

A. Soft Robotic Sleeve Design

The proposed soft robotic sleeve embeds three soft optical sensors (i.e. waveguides) and three soft actuators distributed at equal intervals around the periphery of the device, such that when the robot is wrapped around a colonoscope, the sensors are positioned at 120° apart, as are the actuators (Fig. 1, B). The overall dimensions of the soft robotic sleeve (when fabricated in a flat configuration) are 62 × 118 × 3.5 mm in width, length, and thickness. The inner diameter (ID) of the wrapped sleeve is 19.5 mm and can be mounted around the distal segment of standard commercial colonoscopes, outer diameters (OD) ranging from 9.5 mm to 13.8 mm [31], using a cylindrical shell adapter with an OD of 19.5 mm and an ID equivalent to the size of the chosen scope. The current size of the sleeve enables it to fit around a wide range of colonoscopes while only having to change the size of the adapter, rather than redesigning the sleeve for each specific scope. The sleeve features soft optical sensors, with cores of 100 mm in length and 1 $mm \times 1\ mm$ cross sections, and elliptically-shaped actuators of major axis of 85 mm and a minor axis of 11 mm with an actuation membrane of 0.5 mm (Fig. 2), promoting out-of-plane expansion to ensure no interference of the actuators on the waveguide's light transmission. The robot main body and its actuators are made of Ecoflex™ 00–30 (Smooth-On). The waveguides are constructed using Vytaflex™ 20 (Smooth-On) as optical core, with refractive index (RI) $n_1 = 1.46$, and the surrounding Ecoflex™ 00–30 as cladding, with an RI $n_2 = 1.41$, promoting an angle of total internal reflection θ_c of 74.8° (Fig. 3, A) [32], [33], according to Eq. 1:

$$\theta_c = sin^{-1}(n_2/n_1) \tag{1}$$

Ecoflex™ 00–30 was chosen due to its low RI, serving as cladding and allowing optical light propagation through the sensor core; and its flexibility (Young's modulus, E = 125 kPa) and large stretchability (elongation at break, 900%), serving as an effective soft actuator, capable of large deformations at relatively low pressures to be safe on the colon walls. Vytaflex™ 20 was chosen due to its low viscosity (1,000 cps), allowing for ease in fabrication, and its higher RI with respect to Ecoflex™ 00–30, promoting good light transmission. Using Ecoflex™ 00–30 as the cladding allows applied forces to be effectively transmitted to the Vytaflex™ 20 core region, as quantified by the difference in durometer of the cladding and core materials. Light is transmitted through the cores from an LED (TSHA4400, Vishay Semiconductors) to a photodiode (PD) (SFH 229, OSRAM Opto Semiconductors) mounted at opposite ends of the sleeve (Fig. 2, H). Light is separated into being reflected, transmitted, or absorbed by the material at the interface. Thus, changing the shape of the waveguide externally, or warping the cross section internally (Fig. 3, A–B), will lead to various light intensity loss modes (see Sect. II-E).

B. Soft Robotic Sleeve Modeling

We modeled the soft robotic sleeve along with a colonoscope and surrounding colon tissue using Abaqus (Simulia, Dassault Systems). The properties of Ecoflex™ 00–30 were modeled as an incompressible material using the hyperelastic Yeoh strain energy potential model with coefficients C10 = 17000, C20 = −200, and C30 = 23 [34]. The properties of the colon were

modeled by utilizing an elastic model where Young's modulus for the colon tissue is 5.18 MPa, Poisson's ratio is 0.5, and the density of the colon tissue is approximated at 1040 kg/m^3 [35], [36]. The modeled colon segments have an inner diameter of 40 mm and are 2.5 mm thick [37]. The colonoscope is included to show the full depiction of the device and is modeled as a rigid cylindrical beam, which prohibits actuator expansion along the bottom of the sleeve. A tetrahedral mesh with a quadratic geometric order, hybrid element type, and a universal seed size of 2.5 mm was used on all elements in the simulations, which results in C3D10H elements (10-node quadratic tetrahedron).

C. Soft Robotic Sleeve Fabrication

The device is fabricated flat using a CNC (Computer Numerical Control) machined aluminum mold and subsequently wrapped in a cylindrical shape to fit around standard commercial colonoscopes (see video). The mold has six holes drilled into its sides for inserting metal dowel pins (2 mm diameter and 18 mm length) to leave space for insertion of LEDs and PDs (Fig. 2, A–B). Ecoflex™ 00–30 is poured into the mold, degassed, and cured (20 min at 70° C). The pins are removed, the elastomer is demolded, and the pins are reinserted ensuring a snug fit and leaving the core area exposed to inject Vytaflex™ 20 (Fig. 2, C). The core is injected with a syringe ensuring no inconsistencies (i.e. air bubbles or debris) and is cured over night at room temperature (Fig. 2, D). This process ensures light transmission and a clean optical interface between the core and LEDs/PDs, by avoiding Ecoflex™ 00–30 to be poured between the insert and the core mold. Another layer of Ecoflex™ 00–30 is injected and cured to seal the core off and create a 3 mm thick device with actuator chambers remaining to be sealed (Fig. 2, E). The pins are removed and a 0.5 mm thick layer of Ecoflex™ 00–30 is spin coated at 250 rpm for 30 s and bonded to the sleeve (Fig. 2, F). Excess material is cut away leaving the completed sleeve with sealed actuation chambers (Fig. 2, G). Three LEDs and PDs are inserted into the cavities on each side of the sleeve (Fig. 2, H).

D. Soft Robotic Sleeve Testing and Validation

We fabricated two colonoscope models. One consists of a 19.5 mm diameter Elastosil M4601 (Smooth-On, USA) cylinder. The other is a 19.5 mm flexible tubing (McMaster, USA). This incorporated a cable, tied at the tip via a small incision and running along the outer body of the tubing through acrylic guide rings, to allow manual steering of the colonoscope model. To secure the robot around the colonoscope, the sleeve is first bonded onto a thin piece of fabric using Silpoxy (Smooth-On, USA) and then the fabric is sewn in a cylindrical shape to fit tightly around the diameter of the scope (see video). We built an *in-vitro* setup to validate the sleeve's ability to navigate the colon and provide pressure redistribution upon monitoring excessive contact force. The colon was modeled using a 50 mm diameter cylindrical film of thermoplastic elastomer (TPE) (Stretchlon® 200, Fibre-Glast, USA) bonded to acrylic pedestals. Three force sensors (Tekscan Flexiforce™A401) were bonded to the interior of the colon model (Fig. 10).

E. Soft Optical Sensors Operation

As the soft robotic sleeve navigates in the colon, it will contact the colon walls and bend along with the colonoscope, thus the soft optical sensors will experience light intensity loss

due to these motion inputs. Fig. 3, A and B depict the scattering of light rays that results respectively from contact forces and bending angles altering the shape and/or straining the cross section of a waveguide. The loss mode due to contact forces is most important for our application, as the primary function of our device is to monitor interactions between the colonoscope and the surrounding lumen, and react in case of excessive force concentrations. We measured the output power change P due to: 1) contact forces that alter the shape or cross section of the waveguide, and 2) losses due to bending, which alter the angle of the incident light throughout the waveguide length, using the relationship of the output power of an undeformed waveguide (I_o) to the current measured power through the waveguide (I) as:

$$P = 10log_{10}(I_o/I) \tag{2}$$

where P is the change in output power, read by a PD, whenever there is a loss ($P > 0$) or a gain ($P < 0$) in light intensity. The voltage reading from each PD is output as a current and the signal is sent through a current to voltage converter circuit that amplifies the signal into a readable voltage which is utilized as the light intensity power (P) in Eq. 2. The voltage converter circuit consists of an LM358N op-amp, a 2 MΩ Resistor, and a 4700 pF capacitor (Fig. 3, F).

We characterized and calibrated the embedded sensors (see Sect. III-B) by subjecting them to: *1)* applied contact forces up to 3 N, and *2)* bending angles up to 90°, changing the device orientation by rolling it around its longitudinal axis in a range from 0° to 360° with steps of 40° (Fig. 3, D). The waveguide cores have anisotropic internal features resulting directly from the roughness of the CNC mold used to manufacture the soft robotic sleeve. The fabrication process dictates that the top surface of the waveguides (Fig. 2, D), corresponding to the outer part of the sleeve when wrapped (Fig. 1, B), is smooth as it cures overnight and levels out ideally for minimal roughness (Fig. 3, E). On the contrary, the bottom surface of the waveguides (closest to the endoscope when the sleeve is wrapped) has a roughness matching that of the mold and likewise the sides of the core develop their roughness based on the tool path of the CNC machine. We use these directional discrepancies to our advantage in order to map the device's position and orientation by having a single sensor be multimodal in terms of bending loss being dependant on bending direction and device orientation. These characterizations and sensors redundancy enable discrimination between losses due to contact force and bending, allowing for the latter to be filtered out and enabling to sense one point of contact.

We also note that the expansion of the soft actuators upon pressurization may cause shape alterations of the waveguides channels via a pressure induced force that would be applied laterally in-plane of the sleeve, if the deformation of the actuators was not predominately out of plane. We tested sensors response upon actuators pressurization and discussed its effects on light transmittance in Sect. III-C.

F. Control Platform

The control platform of the soft robotic sleeve is composed of a PC running a Matlab (Mathworks, USA) script that displays a graphical user interface (GUI), controls the inflation of the actuators, and collects real-time input from the PDs. The data collected from

the soft sensor is converted to estimated forces applied to the sleeve by using calibration data from experimental characterizations. The system provides contact force feedback (via visual and/or auditory signals) to the surgeon via the GUI. The three soft actuators are automatically inflated simultaneously upon force detection above a predefined threshold (that can be tuned by the surgeon). The deployment of the soft actuators is controlled using pressure regulators (IT0010–2N, SMC Pneumatics, USA) which can simultaneously monitor the pressure in the system. The actuators can also be pressurized simultaneously or independently upon demand by the surgeon, if deemed necessary during colonoscopy (i.e. to assist during navigation and distend collapsed tissue).

III. Experimental Results and Discussion

A. Soft Robotic Sleeve FEA Results

We simulated the inflation of the soft actuators on: a sleeve free to expand (Fig. 4, A), a sleeve surrounded by colon tissue in a straight configuration (Fig. 4, B), and a sleeve bent at 60° within a surrounding lumen (Fig. 4, C). The propagation of the strain effects of the soft actuators inflation on the waveguide core regions of the sleeve was monitored via our FEA model (Fig. 4, A). In simulations, the strain on the sensors is negligible up to 4.4 kPa, at which point the actuators have expanded out-of-plane by 17.81 mm. At this magnitude of expansion, the actuators will have already established contact with the colon tissue. In order to model the interaction forces between the soft actuators and the colon walls, we included a colon section and monitored reaction strains and stresses on the colon tissue and the displacement of the sleeve actuators (Fig. 4, B). The point on the colon with the maximum stress, resulting from actuator expansion, is plotted along with the rise in the actuator out-of-plane toward the colon wall. Upon actuator contact with colon tissue (at ≈4 kPa), stress on the colon starts to rise, the actuator expansion develops laterally, distributing forces along a larger area, and thus the rise in height slows. Additionally, the soft robotic sleeve was modeled in the colon in a bent configuration to simulate typical positions assumed during colonoscopy (Fig. 4, C). Here, the soft robotic sleeve's capability to reposition and center the colonoscope during navigation within the lumen, by inflating the actuators, is shown. This is particularly relevant in instances when the colonoscope is stuck and pressing on a concentrated area. The maximum level of strain on the colon is similar in the bent and straight configurations.

B. Soft Optical Sensor Characterization

Three soft robotic sleeve prototypes were fabricated and tested. Testing was performed using an Instron testing machine (5943 Instron, USA). PDs voltage signals are calibrated and collected by the Instron in real time during the test. Although the fabrication process yields consistent results, an initial calibration is carried out for each individual disposable sleeve before validation testing (Sect. III-D1) to ensure proper device functionality.

1) Contact Force Characterization: The three waveguides (WG-A, WG-B, and WG-C) were subjected to an applied force via a $5\ mm \times 5\ mm$ cross section indenter at nine different locations (Fig. 3, C), three times each. The sleeve was aligned to these locations using custom designed acrylic platforms (insets of Fig. 5). The force was monitored using

the Instron load cell (Instron 2530–50N, USA). Force was applied from the top surface of the sleeve down to the bottom surface of the cross section of the waveguide, by moving the indenter downwards at 1 mm/min for 2.5 mm. The sleeve was tested both in a flat (Fig. 5, D) and in a wrapped (Fig. 5, A–C) configutation to monitor the sensitivity of the waveguides as manufactured and in their intended layout (i.e. wrapped around a colonoscope), to determine if this resulted in any difference in repeatability or loss characteristics. The sleeve responded similarly when flat and wrapped, suggesting that functionality is not affected after mounting the device in the desired configuration. The plots show the three waveguides WG-A, WG-B, and WG-C response to applied force in a range from 0 to 3 N in the different testing locations, leading to losses up to 15 dB, with a maximum of 13% difference between the sleeves tested.

2) Bending Angle Characterization: We characterized the soft sensors response to bending, and its correlation to the roughness of the waveguides, by subjecting the sleeve to bending angles up to 90° (using the Elastosil cylinder), changing the device orientation by rolling it around its longitudinal axis in a range from 0° to 360° with steps of 40° (Fig. 3, D). Results are shown in Fig. 6 where the sleeve was oriented such that four of the nine different tested bending angles are shown: 0° (Fig. 6, A), 40° (Fig. 6, B), 80° (Fig. 6, C), and 120° (Fig. 6, D). In Fig. 6, A, WG-A and WG-C experience more loss than WG-B due to WG-B bending plane being primarily on its outer (i.e. smooth) surface (Fig. 3, E). Likewise, in Fig. 6, B, WG-B experiences less loss due to being in the same position with respect to the bending plane. Further, in Fig. 6, C, WG-B and WG-C are positioned such that the bending direction causes less loss than WG-A and, once again, the dual modality of the sensors is exhibited. The remaining bending orientations (i.e. 120°–160°–200°, and 240°–280°–320°) result in similar loss responses with only the specific waveguide experiencing the loss changing, depending on its position with respect to the bending plane; i.e., at 120° (Fig. 6, D), WG-A, WG-B, and WG-C respond respectively as WG-C, WG-A, and WG-B at 0° (Fig. 6, A). This carries for all other orientations apart from minor discrepancies due to the fabrication process. By monitoring the three WGs simultaneously, the intensity loss due to bending can be discerned from contact forces by taking advantage of the redundancy that the sensors provide at each bending orientation. The sleeve's aim is not to track its bending, orientation, nor shape, but rather filter bending loss while continuing to monitor contact force interactions, taking advantage of sensor redundancy (see Sect. III-D1).

C. Soft Actuators Characterization

The soft actuators were characterized to determine their output blocked force and their effects on the waveguides upon inflation. The pressure applied to inflate each actuator was monitored using a pressure sensor (HSCDANN160MGAA5, Honeywell International, Inc). This signal is calibrated and collected by the Instron in real time during the test.

1) Actuator Expansion Effects on Soft Sensors: Using the test setup shown in the inset of Fig. 7 D, the actuators effect on the waveguides was tested. Fig. 7 shows that the free expansion of the actuators (1, 2, and 3 as shown in Fig. 3) does not affect the transmittance of light through the waveguides until ≈3 kPa of pressurization. Inflating the actuators beyond 3 kPa resulted in losses up to about 2 dB depending on the proximity of the

WG to the inflated actuator with the waveguides adjacent to the actuators experiencing the largest loss. WG-A presents a larger loss than the other waveguides when actuator 1 (Fig. 7, A) is expanded and less when actuator 3 is expanded (Fig. 7, C). This is because WG-A is on the far edge of the sleeve and not bonded to the portion of the sleeve adjacent to actuator 3, as a result of the flat fabricated sleeve being wrapped. It is important to note that when all actuators are expanded simultaneously, the loss still begins after 3 kPa.

Soft actuators expansion upon pressurization was tested. Given a normal colon lumen ID of ≈45 mm, each actuator would need to expand ≈10 mm to contact the colon walls and redistribute force concentrations or aid during navigation. Fig. 7, D shows that the pressure required to reach ≈10 mm of actuator expansion is less than 2.5 kPa (i.e. smaller than the critical value of 3 kPa). Because there are three actuators, even if the device is not centered in the lumen, at least one of the actuators will contact tissue before 3 kPa of pressure is required. Thus, in the working range, there will be no loss due to actuator expansion. In case the sleeve is located in an area of the colon with a larger internal diameter, we determined the maximum free expansion actuation height (while remaining at safe operation pressures in the colon) of the actuators to be greater than 2 cm; thus, the sleeve will contact the colon with minimal losses prior to surpassing 3 kPa. Further, upon actuators inflation, triggered by excessive contact forces, the force does not need to be monitored until after the actuators are deflated, according to the desired clinical workflow (Fig. 1).

2) Actuator Blocked Force Testing: The sleeve was setup with a compression anvil with a plate constraining actuators expansion to evaluate blocked force (Fig. 8, B). The testing was conducted until 14 kPa of pressure was input. The maximum blocked force for the soft actuators is 15 N (Fig. 8, A). During this test, actuators pressurization caused negligible (less than 5%) loss through the waveguides.

D. Validation

The soft robotic sleeve was tested using the two validation setups described in Sect. II-C to evaluate sensing and control capabilities and demonstrate the device functionality *in-vitro*.

1) Sensor Control Validation: During the operation of the sleeve, the estimated force applied to each sensor is monitored and used to determine when the actuators are deployed. The threshold for actuator deployment is set at 1.5 N via the GUI (this can be changed as desired by the user). The sleeve is placed in a custom 3D-printed jig to display its full range of capabilities of estimating force, filtering bending losses, and reactively deploying actuators (Fig. 9, A–H). The test (see video) begins with the sleeve in a straight configuration with an arbitrary force applied manually to WG-B (Fig. 9, A). As the estimated force surpasses 1.5 N, the actuators are deployed until the force is released (Fig. 9, B). Then, the sleeve is bent at 90°, using the jig. The system filters the sensor loss due to bending (Fig. 9, C) using the control platform (Sect. II-F) and exploits the calibration data from the experimental characterizations to establish a new baseline output power in the bent configuration to calculate subsequent losses due to contact. The Instron is moved to contact WG-C and a known force is applied. The estimated force is plotted with the Instron data as the actuators inflate past the appropriate threshold (Fig. 9, D–F). The minor discrepancy

between the estimated and applied force derives from the difference in accuracy between the Instron load cell and our optical sensor. Finally, the Instron is moved away and the actuators deflate as the device continues monitoring forces (Fig. 9, G–H).

2) In-Vitro Validation: We tested the sleeve navigation and force redistribution capabilities (see Fig. 10 and video) in the *in-vitro* setup (Sect. II-C). The surgical workflow is: *1)* The colonoscope is inserted and advanced manually (as conventionally). *2)* During navigation, the soft optical sensors monitor the force exerted by the colonoscope onto the colon wall. The scope contacts the first bend in the colon and an excess force is exerted (Fig. 10, A). *3)* The force is redistributed by inflating the soft actuators (Fig. 10, B). *4)* The colonoscope is advanced through the critical area of force concentration exploiting the navigation aid provided by the inflated soft actuators (Fig. 10, C). *5)* Critical area is passed, actuators are deflated, sensors continue monitoring forces, and navigation continues (Fig. 10, D). We used a general purpose lubricant to facilitate insertion and navigation, as commonly done in colonoscopy. To quantitatively measure the force redistribution in Fig. 10, B, this step was tested separately to accommodate the force sensors more effectively while accurately repeating the excessive force contact on the lumen wall (Fig. 10, E) and deploying the soft actuators to lower the pressure (Fig. 10, F). The initial contact force was 4.7 N, concentrated on a single sensor (Fig. 10, E). Upon inflation of the actuators, the force on that same sensor decreases to 1.9 N, while the other two sensors increased from 0 N to 2.6 N and 0.6 N, thus showing force redistribution along a circumference (Fig. 10, F).

IV. Conclusion

We present a proof-of-concept of a soft robotic sleeve with embedded soft optical sensors and soft actuators, which can provide sensor feedback and additional actuation functionalities to improve navigation and safety in colonoscopy. We introduce a low-cost manufacturing method to enable integration of sensing and actuation capabilities in a disposable endoscopic add-on. The device is fabricated flat and then wrapped around a colonoscope and adapted to different scope diameters. The design is informed by FEA and supported by experimental testing results. We have modeled the soft robotic sleeve upon actuator expansion in free motion and inserted in a colon lumen to evaluate its interaction with the anatomy. The operation of the soft optical sensors is characterized with calibration and validation tests. Sensors' loss modes were investigated during contact forces, bending motions, and actuator inflation. We demonstrated that the sleeve is able to discern bending orientation from contact interactions and can successfully monitor contact force between the colon and the colonoscope. The device is designed to be positioned around the colonoscope distal segment, where force concentrations reach high peak values during navigation. This system can help steer the colonoscope while also diminishing force outputs onto the colon wall compared to standard colonoscopy and other robotic approaches. To power the sleeve, three fluidic lines are integrated along the scope. To prevent tangling, actuation lines pass through disposable tube holders, which allow sliding to facilitate scope bending. Future work will focus on scaling down the sleeve thickness and outer diameter to facilitate navigation throughout the entire colon (i.e. up to the cecum), using soft lithography processes [38]. The system will be integrated onto a commercial colonoscope to investigate

its efficacy in colonoscopy in an *ex-vivo* model (i.e. porcine colon explants). Pressurization will be controlled by pressure regulators connected to a pressure and power source at the endoscopy column, outside the patient's body.

Supplementary Material

Refer to Web version on PubMed Central for supplementary material.

Acknowledgments

Research reported in this publication was supported by the National Institute of Biomedical Imaging and Bioengineering of the National Institutes of Health under award number R21EB029154. The content is solely the responsibility of the authors and does not necessarily represent the official views of the National Institutes of Health.

References

[1]. Bonjer HJ et al., "A randomized trial of laparoscopic versus open surgery for rectal cancer," New England Journal of Medicine, vol. 372, no. 14, 2015.

[2]. Siegel RL, Miller KD, and Jemal A, "Cancer statistics, 2020," CA: A Cancer Journal for Clinicians, vol. 70, no. 1, 2020.

[3]. Loeve A, Breedveld P, and Dankelman J, "Scopes too flexible and too stiff," IEEE Pulse, vol. 1, no. 3, pp. 26–41, 11 2010. [PubMed: 21097368]

[4]. Valdastri P, Simi M, and Webster RJ, "Advanced technologies for gastrointestinal endoscopy," Annual Review of Biomedical Engineering, vol. 14, 2012.

[5]. Franco DL, Leighton JA, and Gurudu SR, "Approach to incomplete colonoscopy: New techniques and technologies," Gastroenterology and Hepatology, vol. 13, no. 8, 2017.

[6]. Rutter MD, Nickerson C, Rees CJ, Patnick J, and Blanks RG, "Risk factors for adverse events related to polypectomy in the english bowel cancer screening programme," Endoscopy, vol. 46, no. 2, 2014.

[7]. Reumkens A, Rondagh EJ, Bakker CM, Winkens B, Masclee AA, and Sanduleanu S, "Post-colonoscopy complications: A systematic review, time trends, and meta-analysis of population-based studies," American Journal of Gastroenterology, vol. 111, no. 8, 2016.

[8]. Laanani M, Coste J, Blotière PO, Carbonnel F, and Weill A, "Patient, Procedure, and Endoscopist Risk Factors for Perforation, Bleeding, and Splenic Injury After Colonoscopies," Clinical Gastroenterology and Hepatology, vol. 17, no. 4, pp. 719–727, 3 2019. [PubMed: 30099110]

[9]. Joseph DA, Meester RG, Zauber AG, Manninen DL, Winges L, Dong FB, Peaker B, and van Ballegooijen M, "Colorectal cancer screening: Estimated future colonoscopy need and current volume and capacity," Cancer, vol. 122, no. 16, 2016.

[10]. Wernli KJ, Brenner AT, Rutter CM, and Inadomi JM, "Risks Associated with Anesthesia Services during Colonoscopy," Gastroenterology, vol. 150, no. 4, 2016.

[11]. Boškoski I and Costamagna G, "Endoscopy robotics: Current and future applications," Digestive Endoscopy, vol. 31, no. 2, 2019.

[12]. Mylonas GP, Vitiello V, Cundy TP, Darzi A, and Yang GZ, "CYCLOPS: A versatile robotic tool for bimanual single-access and natural-orifice endoscopic surgery," in Proceedings - IEEE International Conference on Robotics and Automation, 2014.

[13]. Arkenbout EA, Henselmans PW, Jelínek F, and Breedveld P, "A state of the art review and categorization of multi-branched instruments for NOTES and SILS," Surgical Endoscopy, vol. 29, no. 6, 2015.

[14]. Beyna T, Schneider M, Pullmann D, Gerges C, Kandler J, and Neuhaus H, "Motorized spiral colonoscopy: A first single-center feasibility trial," Endoscopy, vol. 50, no. 5, 2018.

[15]. Eickhoff A, Jakobs R, Kamal A, Mermash S, Riemann JF, and van Dam J, “In vitro evaluation of forces exerted by a new computer-assisted colonoscope (the NeoGuide Endoscopy System),” Endoscopy, vol. 38, no. 12, 2006.

[16]. Rösch T, Adler A, Pohl H, Wettschureck E, Koch M, Wiedenmann B, and Hoepffner N, “A motor-driven single-use colonoscope controlled with a hand-held device: a feasibility study in volunteers,” Gastrointestinal Endoscopy, vol. 67, no. 7, 2008.

[17]. Yeung BPM and Chiu PWY, “Application of robotics in gastrointestinal endoscopy: A review,” World Journal of Gastroenterology, vol. 22, no. 5, 2016.

[18]. Appleyard MN, Mosse CA, Mills TN, Bell GD, Castillo FD, and Swain CP, “The measurement of forces exerted during colonoscopy,” Gastrointestinal Endoscopy, vol. 52, no. 2, 2000.

[19]. Case JC, White EL, and Kramer RK, “Soft material characterization for robotic applications,” Soft Robotics, vol. 2, no. 2, 2015.

[20]. Christensen MB, Oberg K, and Wolchok JC, “Tensile properties of the rectal and sigmoid colon: a comparative analysis of human and porcine tissue,” SpringerPlus, vol. 4, no. 1, 2015.

[21]. Manwell T, Vitek T, Ranzani T, Menciassi A, Althoefer K, and Liu H, “Elastic mesh braided worm robot for locomotive endoscopy,” in 2014 36th Annual International Conference of the IEEE Engineering in Medicine and Biology Society, EMBC 2014, 2014.

[22]. Tumino E, Sacco R, Bertini M, Bertoni M, Parisi G, and Capria A, “Endotics system vs colonoscopy for the detection of polyps,” World Journal of Gastroenterology, vol. 16, no. 43, 2010.

[23]. Pfeffer J, Grinshpon R, Rex D, Levin B, Rösch T, Arber N, and Halpern Z, “The Aer-O-Scope: Proof of the concept of a pneumatic, skill-independent, self-propelling, self-navigating colonoscope in a pig model,” Endoscopy, vol. 38, no. 2, 2006.

[24]. Garbin N, Wang L, Chandler JH, Obstein KL, Simaan N, and Valdastri P, “A disposable continuum endoscope using piston-driven parallel bellow actuator,” in 2018 International Symposium on Medical Robotics, ISMR 2018, vol. 2018-1, 2018.

[25]. Yamamoto H, Sekine Y, Sato Y, Higashizawa T, Miyata T, Iino S, Ido K, and Sugano K, “Total enteroscopy with a nonsurgical steerable double-balloon method,” Gastrointestinal Endoscopy, vol. 53, no. 2, 2001.

[26]. Becker S, Ranzani T, Russo S, and Wood RJ, “Pop-up tissue retraction mechanism for endoscopic surgery,” IEEE International Conference on Intelligent Robots and Systems, vol. 2017-Septe, no. Iros, pp. 920–927, 2017.

[27]. Ranzani T, Russo S, Schwab F, Walsh CJ, and Wood RJ, “Deployable stabilization mechanisms for endoscopic procedures,” in Proceedings - IEEE International Conference on Robotics and Automation, 2017.

[28]. Davidson T, Levi M, Levy I, and Gilreath M, “Endoscope with Integrated Sensors,” United States Patent US2015/0099926A1, 2015.

[29]. Watanabe T, Iwai T, Fujihira Y, Wakako L, Kagawa H, and Yoneyama T, “Force sensor attachable to thin fiberscopes/endoscopes utilizing high elasticity fabric,” Sensors (Switzerland), vol. 14, no. 3, 2014.

[30]. Naghibi H, Gifari MW, Hoitzing W, Lageveen JW, Van As DM, Stramigioli S, and Abayazid M, “Development of a multi-level stiffness soft robotic module with force Haptic feedback for endoscopic applications,” in Proceedings - IEEE International Conference on Robotics and Automation, vol. 2019-5, 2019.

[31]. “Olympus Corp., “Olympus Gastroenterology Products”, Internet: https://www.olympus-europa.com/medical/en/Products-and-Solutions/Products/Gastroenterology/Colonoscopes.html, [10, 23, 2020].”

[32]. Zhao H, O’Brien K, Li S, and Shepherd RF, “Optoelectronically innervated soft prosthetic hand via stretchable optical waveguides,” Science Robotics, vol. 1, no. 1, p. eaai7529, 2016. [PubMed: 33157858]

[33]. Teeple CB, Becker KP, and Wood RJ, “Soft Curvature and Contact Force Sensors for Deep-Sea Grasping via Soft Optical Waveguides,” International Conference on Intelligent Robots and Systems (IROS), pp. 1621–1627, 2018.

[34]. Steck D, Qu J, Kordmahale SB, Tscharnuter D, Muliana A, and Kameoka J, “Mechanical responses of Ecoflex silicone rubber: Compressible and incompressible behaviors,” Journal of Applied Polymer Science, vol. 136, no. 5, pp. 1–11, 2019.

[35]. Christensen MB, Oberg K, and Wolchok JC, “Tensile properties of the rectal and sigmoid colon: a comparative analysis of human and porcine tissue,” SpringerPlus, vol. 4, no. 1, 2015.

[36]. Choi AP and Zheng YP, “Estimation of Young’s modulus and Poisson’s ratio of soft tissue from indentation using two differentsized indentors: Finite element analysis of the finite deformation effect,” Medical and Biological Engineering and Computing, vol. 43, no. 2, 2005.

[37]. Wiesner W, Mortelé KJ, Ji H, and Ros PR, “Normal colonic wall thickness at CT and its relation to colonic distension,” Journal of Computer Assisted Tomography, vol. 26, no. 1, pp. 102–106, 2002. [PubMed: 11801911]

[38]. Russo S, Ranzani T, Walsh CJ, and Wood RJ, “An Additive Millimeter-Scale Fabrication Method for Soft Biocompatible Actuators and Sensors,” Advanced Materials Technologies, vol. 2, no. 10, pp. 1–12, 2017.

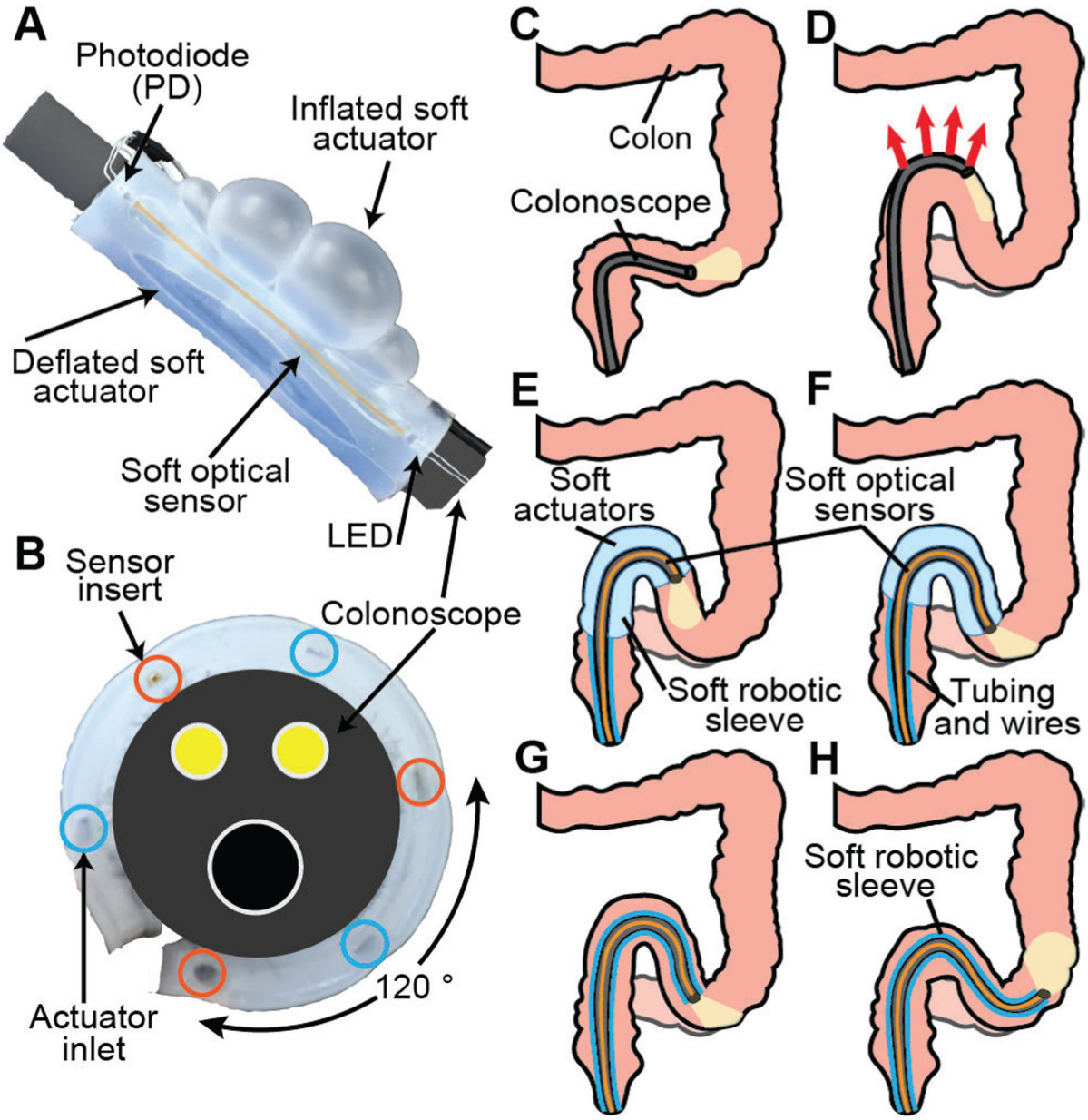

Fig. 1.

A) Soft robotic sleeve wrapped around a colonoscope model. B) Soft sensor inserts and soft actuator pneumatic lines locations. C)-D) Current challenges in endoscopic navigation and E)-H) envisaged clinical workflow of the proposed device. C) Ideal case: colonoscope following the curves of the colon. D) In practice: the scope pushes against the colon and stretches it, applying excessive force. E) The soft robotic sleeve senses the excessive force concentration (using soft optical sensors) and redistributes it on a larger area (by deploying soft actuators). F) The colonoscope is advanced exploiting the navigation aid provided by the soft actuators. G)-H) The actuators are deflated, the sensors continue monitoring interaction forces, and the scope continues navigation.

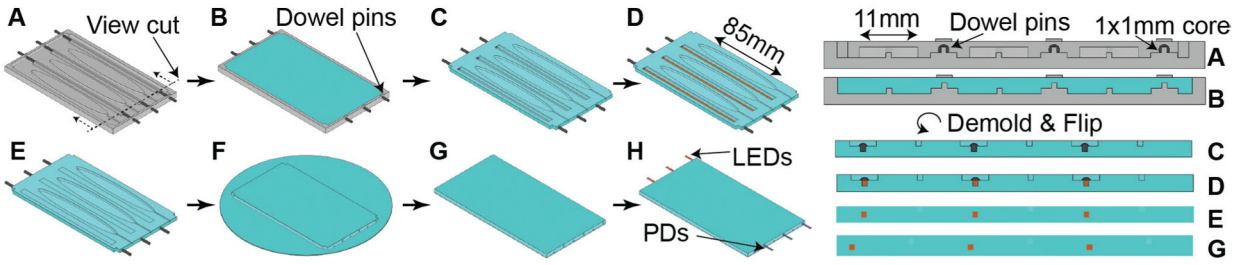

Fig. 2.

Soft robotic sleeve fabrication (left) and corresponding cross sections (right). A) Sleeve mold with metal dowel pins inserted. B) Ecoflex™ 00–30 poured into mold, degassed, and cured. C) Pins removed, Ecoflex™ 00–30 demolded, and pins reinserted. D) Vytaflex™ 20 injected into waveguide core cavities. E) Ecoflex™ 00–30 injected to seal off core region. F) Pins removed and Ecoflex™ 00–30 is spin coated and bonded to the sleeve to seal the actuation chambers. G) Excess material is removed. H) LEDs and PDs insertion for light transmittance and detection through the waveguide cores.

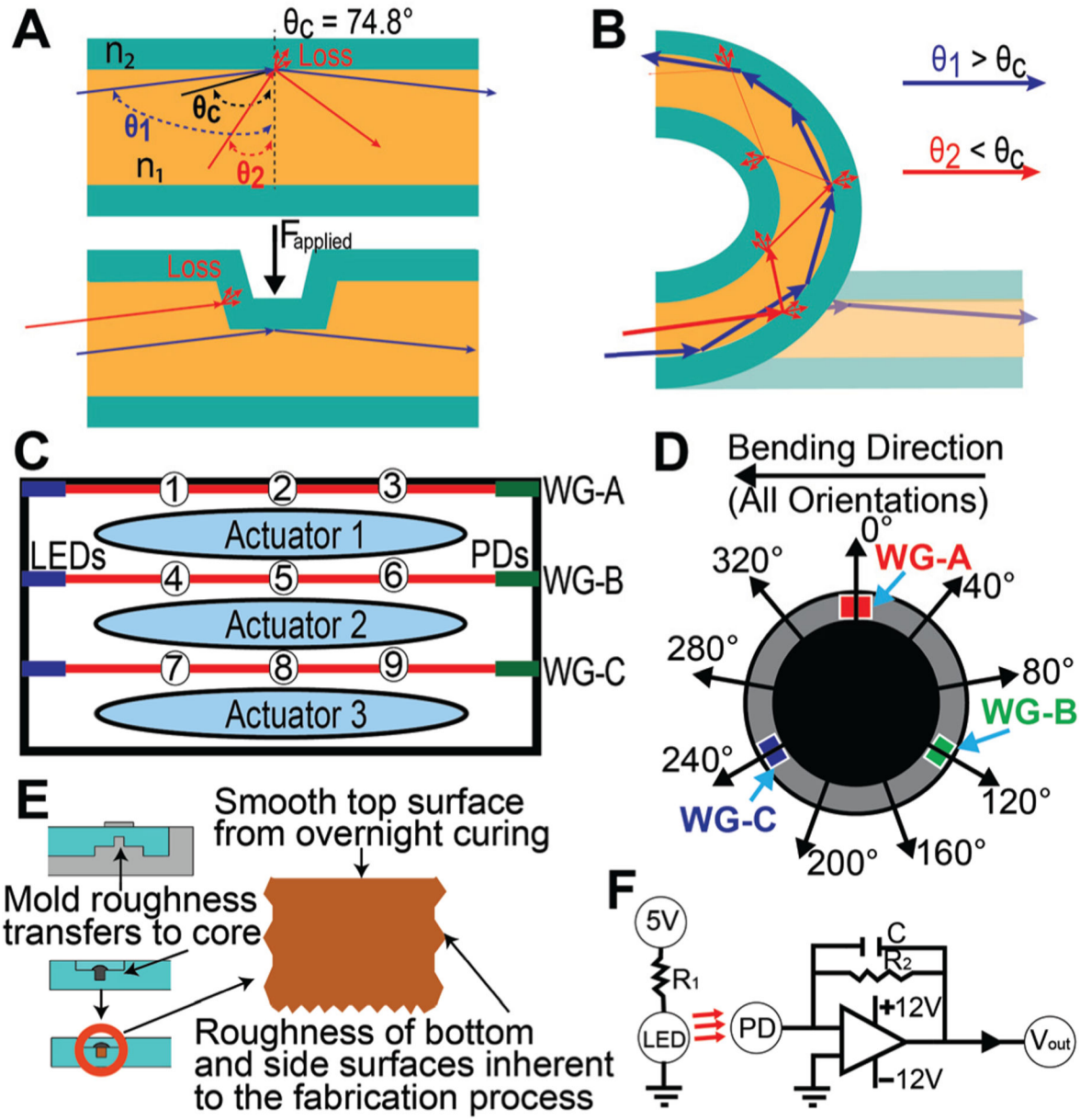

Fig. 3.

A) Angle of total internal reflection (top) and contact force altering the incident light angle (bottom), causing light intensity losses. B) Effect of bending on light transmission. C) Layout of contact force testing positions. D) Orientation diagram for bending direction testing. E) Depiction of fabrication processes determining the roughness of the core region. F) Circuit schematic for the voltage output of the PDs.

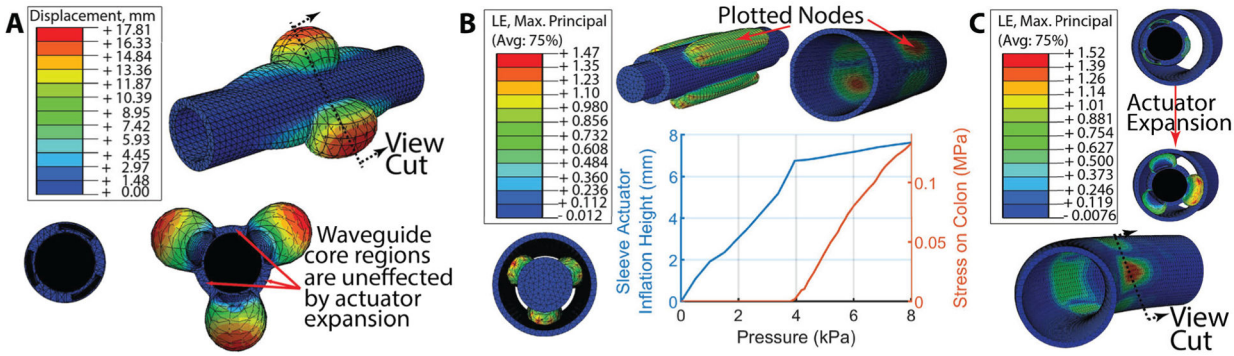

Fig. 4.

Soft robotic sleeve FEA. A) Free expansion height of the actuators at 4.4 kPa (top right) and shape change of the cross section of the sleeve in the plane of maximum expansion (bottom) where there is negligible strain in the waveguide cores. B) Sleeve mounted on colonoscope and surrounded by colon in a straight layout, showing actuator expansion strain (bottom left) and actuator shape and colon strain (top right). On the bottom right, plot depicting the displacement of an actuator node and the resulting stress on a node on the colon. C) Sleeve mounted on colonoscope and surrounded by colon in a bent layout, showing actuator inflation and alignment (top right) and the strain on the colon along the plane of maximum stress.

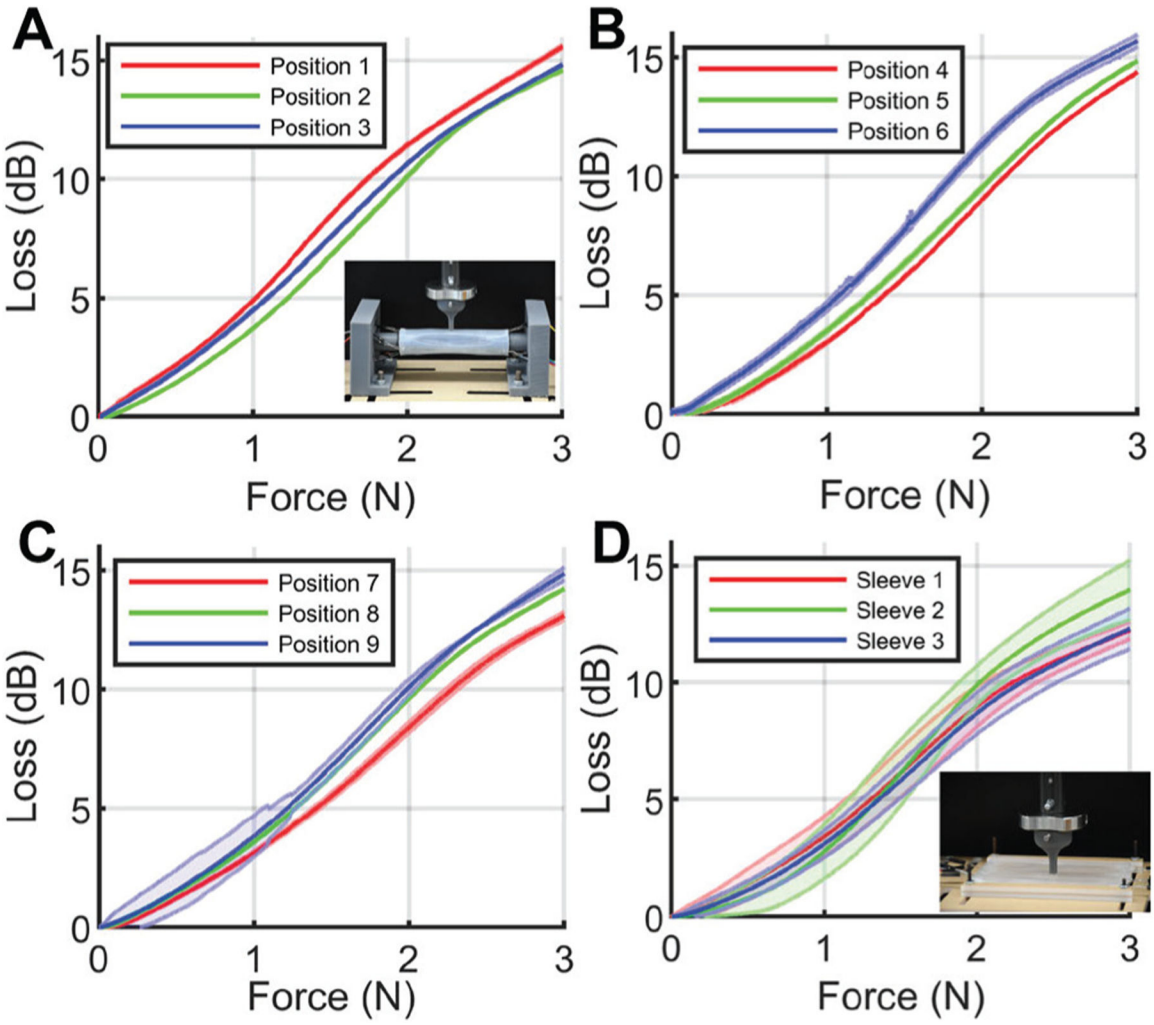

Fig. 5.

Contact force characterization up to 3 N in the wrapped configuration on A) WG-A, B) WG-B, and C) WG-C as well as D) in the flat configuration on the center positions (2, 5, and 8) of each waveguide for each of the three sleeves tested. Please refer to Fig. 3 C for testing positions locations. The solid line is the mean value and the shaded area represents one standard deviation computed on one prototype for each location, tested three times each (A-C) and computed on three prototypes for each location (three per sleeve), tested three times each (D).

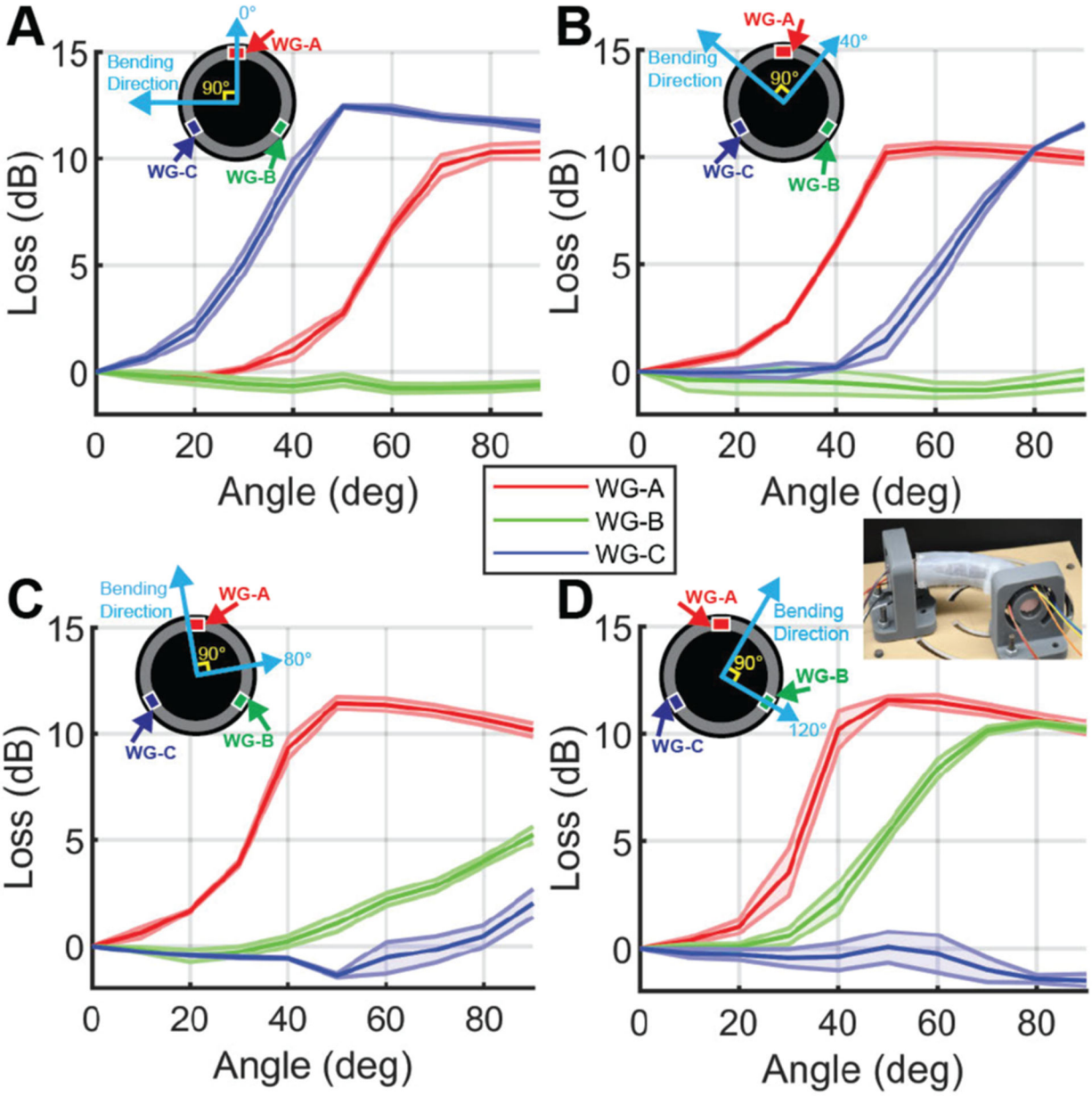

Fig. 6.

Bending loss of sleeve bent at orientations: A) 0°, B) 40°, C) 80°, and D) 120°. The solid line is the mean value and the shaded area is one standard deviation computed on one prototype for each orientation, tested three times each. Please refer to Fig. 3, D for the overall schematic of bending direction testing.

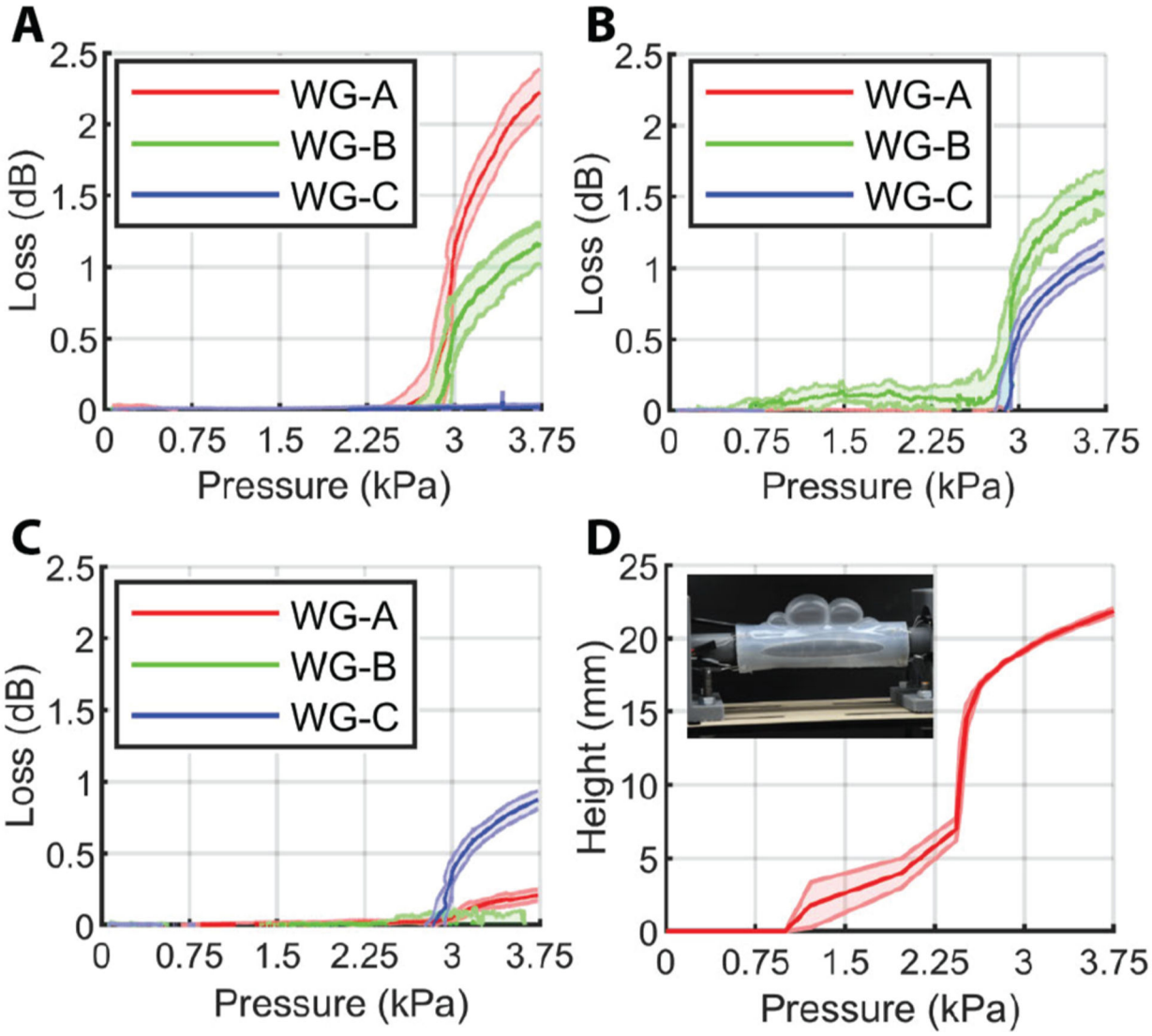

Fig. 7.

Effects of the free expansion of A) Actuator 1, B) Actuator 2, and C) Actuator 3 on the WGs light transmittance. D) Expansion height of the actuators under applied pressures. The solid line is the mean value and the shaded area represents one standard deviation computed on one prototype for each waveguide (A-C) and on one actuator (D), tested three times each.

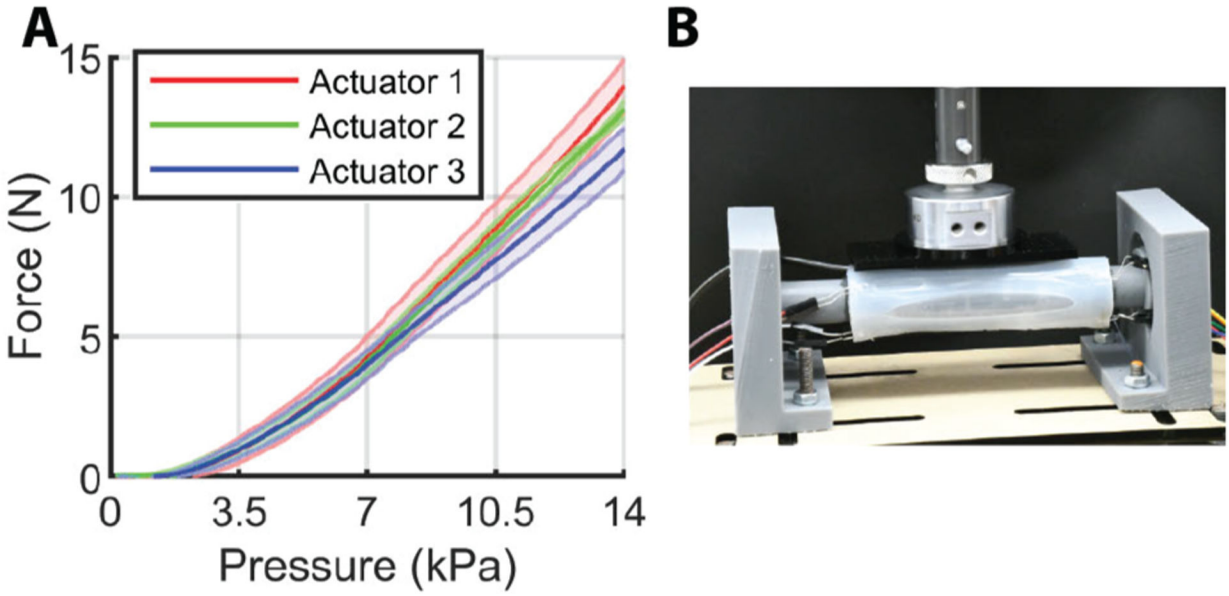

Fig. 8.

A) Force outputs of soft actuators and B) testing platform. The solid line is the mean value and the shaded area is one standard deviation computed on one prototype for each actuator, tested three times each.

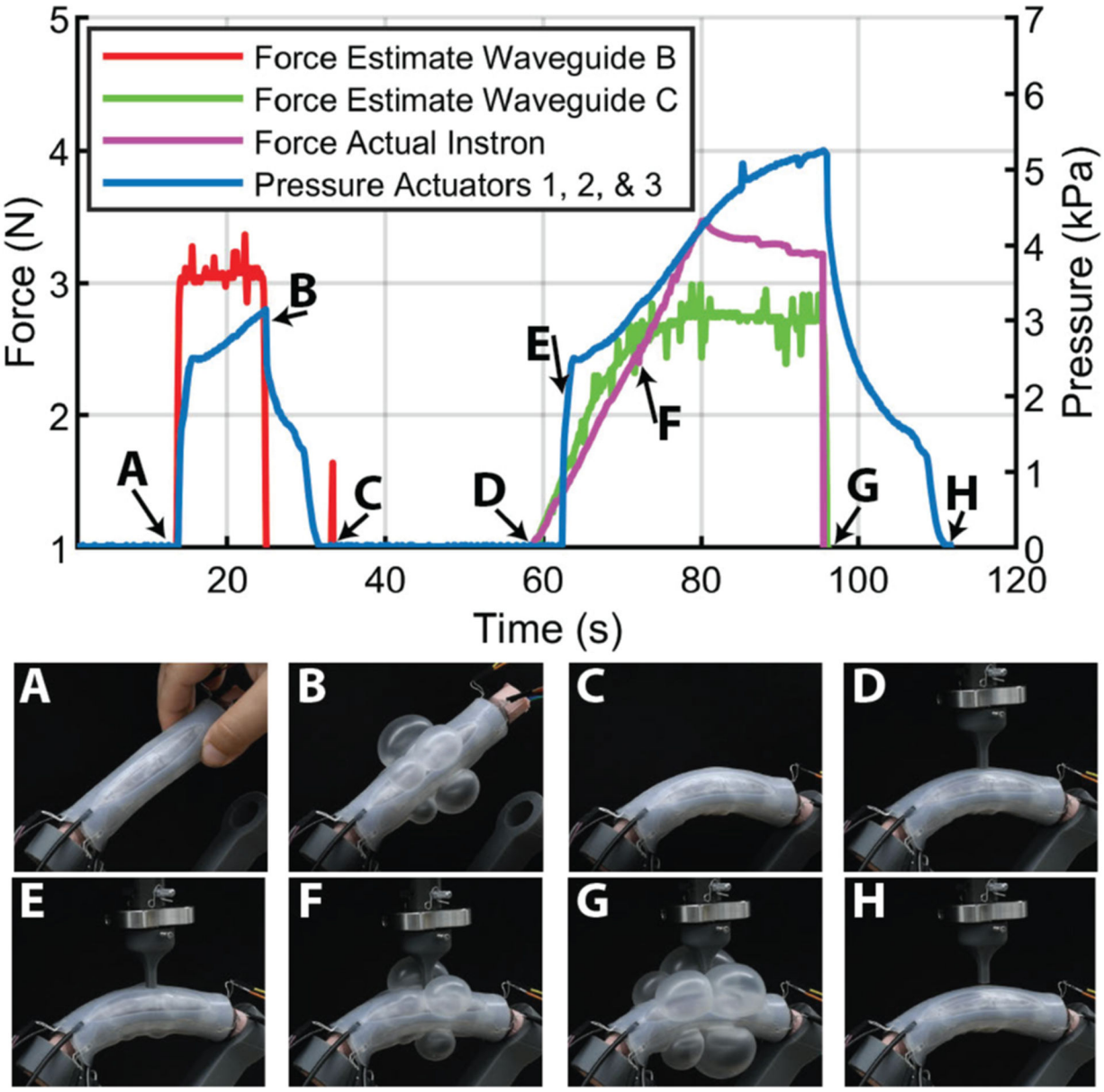

Fig. 9.

Validation of the sleeve's ability to monitor contact force, filter bending loss, and deploy actuators when forces greater than a specified threshold are applied. A) Sleeve is pressed with a finger and estimated force is predicted by WG-B resulting in the deployment of the soft actuators. B) Pressure is released and the actuators deflate. C) Sleeve is bent, our control platform filters the loss, resulting in no actuators inflating. D) Instron contacts WG-C, applying force. E) Estimated force on WG-C surpasses threshold and actuators are deployed. F) Sleeve continues monitoring contact force as actuators continue to expand. G) Force is released and pressure is removed. H) System returns to baseline.

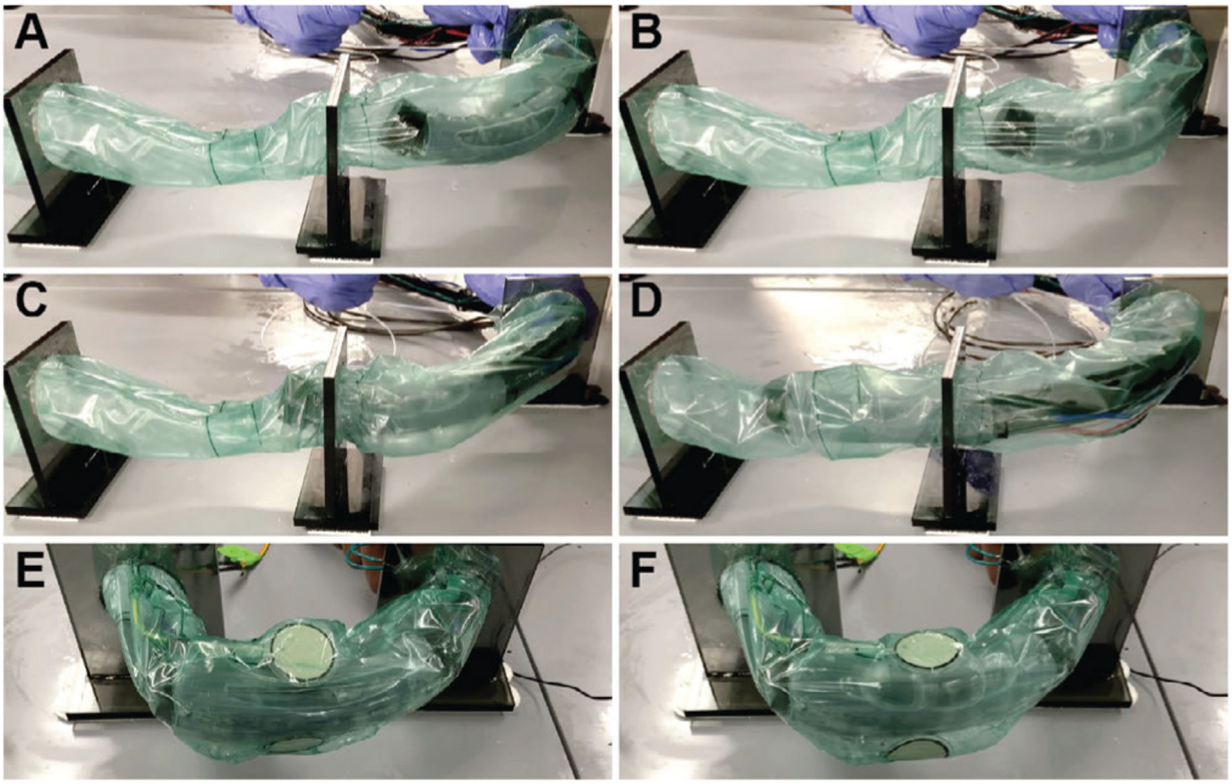

Fig. 10.

In-vitro test. A)-D) Navigation. E)-F) Force redistribution. A) The colonoscope model applies a force on the lumen wall. B) The actuators inflate to redistribute the force. C) The sleeve moves through the critical area of excessive force concentration. D) The actuators are deflated and the system continues navigation. E) Measurement of a concentrated force and F) redistribution via actuators expansion.